Contrast in the Boundary Layer Convergence Lines at Desert−Oasis Border with Different Vegetation Gradient

Zimeng Zheng[1], Zhiyong Meng[1*], Quxin Cui[1], Yipeng Huang[2], Xuefeng Meng[3]

[1]Department of Atmospheric and Oceanic Sciences, School of Physics, and China Meteorological Administration Tornado Key Laboratory, Peking University, Beijing, China

[2]Xiamen Key Laboratory of Straits Meteorology, Xiamen Meteorological Bureau, Xiamen, China

[3]Inner Mongolia Meteorological Observatory, Hohhot, China

*Corresponding author: Zhiyong Meng, zymeng@pku.edu.cn

【Abstract】

Motivated by an observed asymmetry in boundary layer convergence lines (BLCLs) between the Kubuqi and Ulan Buh desert borders of the Hetao Oasis in northern China, this work aims to document the differences in BLCL frequency and convective initiation and their potential drivers. Using radar, surface Automatic Weather Station, and reanalysis data in June–August from 2012 to 2022, we found that the Kubuqi border had more frequent, earlier-forming, and more convective BLCLs, whereas the Ulan Buh border had fewer, shorter-lived, and more tortuous ones. These contrasts were associated with sharper vegetation and thermal gradients, higher Bowen ratio, and a more favorable background wind on the Kubuqi side. Our findings demonstrate that BLCL behavior is highly sensitive to surface, flow, and terrain heterogeneity, even around a single oasis.

【Key Points】

1. BLCLs over the sharper vegetation gradient are more frequent, stronger, more linear, longer-lived, and trigger more convection.
2. BLCLs over the desert with a higher Bowen-ratio form earlier and move farther into the desert associated with faster surface warming.
3. Local terrain exerts opposite impacts on the background wind critical for BLCL formation over the two deserts.

【Plain language summary】

In summer afternoons, winds from the desert and the oasis often meet near their border over the desert side to form convergence lines, pushing air upward to form clouds and sometimes severe storms. These meeting areas are affected by differences in vegetation, the shape of the land, and the overall weather patterns. This study looked at the different behaviors of convergence lines over two deserts that are adjacent to one same oasis in northern China, and the potential underlying physical reasons. Results showed that convergence lines often form along the border of the Oasis over Kubuqi Desert but less so over Ulan Buh Desert. It was found that the temperature difference is larger between the oasis and Kubuqi Desert, creating more favorable conditions for convergence lines. In addition, stronger background winds from Kubuqi Desert do not destroy these lines. In contrast, convergence lines over the Ulan Buh Desert are fewer, weaker, shorter-lived, and more twisted. Some form when short lines merge together. Understanding where and why these lines form helps predict local storms and rainfall in desert–oasis regions, which is important for farming, water management, weather safety, and desert afforestation in arid/semiarid places like Hetao.

【Keywords】 Boundary layer convergence line, vegetation heterogeneity, Background wind, temperature gradient, desert–oasis border, mountain blocking

1. Introduction

Boundary layer convergence lines (BLCLs) often form in heterogeneous surface regions, parallel to the border, and are one of the most important lifting mechanisms for convection initiation (CI). The effects of heterogeneous vegetation on BLCLs and convection have drawn wide attention (Huang et al. 2019; Klein & Taylor, 2020; Yuan et al., 2020; Huang et al. 2022; Chug et al., 2023; Liu et al. 2023; Meng et al., 2024). Previous studies have examined BLCLs and their related convection using in situ measurements, satellite observations, and weather radar data, generally focusing on a single type of vegetation border.

Beyond observational studies, numerous idealized numerical experiments have explored how surface heterogeneity influences BLCLs and CI. Large-eddy and cloud-resolving simulations consistently indicate that the sharpness and spatial scale of surface-flux contrasts play a critical role in organizing low-level convergence, cloud development, and the likelihood of CI (Kang and Bryan 2011; Rieck et al. 2014; Hohenegger and Stevens 2018). These studies provide a clear physical framework linking land-atmosphere coupling to mesoscale circulations.

However, as emphasized by Bou-Zeid et al. (2020), surface heterogeneity remains a persistent challenge in boundary-layer meteorology. Conclusions from idealized frameworks may not directly translate to real-world environments characterized by complex terrain, fragmented land cover, and variable background flow. Consequently, how differences in the magnitude of vegetation gradient manifest in observed BLCL characteristics under realistic conditions remains poorly understood.

In Inner Mongolia, China, the Hetao irrigation oasis is bordered by Kubuqi Desert to the south and Ulan Buh Desert to the southwest (Figure 1a). The border between the Hetao Oasis and Kubuqi Desert follows the Yellow River and is sharp. However, the Hetao Oasis and Ulan Buh Desert cannot be divided by a single line. It is a transition zone where oases, deserts, and lakes coexist, and the underlying surface gradually changes from oasis to desert.

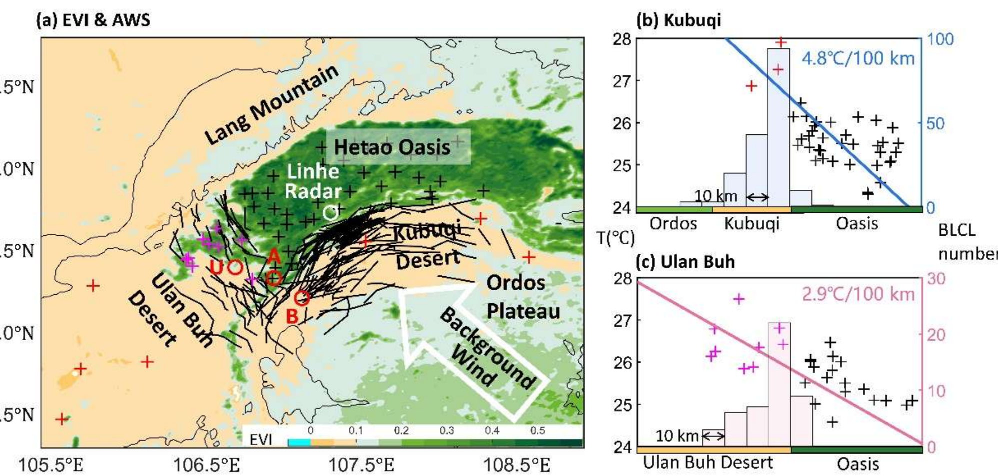

Figure 1. (a) Distribution of BLCLs (black lines) at formation. Shading: Enhanced Vegetation Index (EVI). '+': surface Automatic Weather Station (AWS) locations (black for oasis, red for desert, purple for transition zone). Red open circles: sites A, B, and U (flux observations in Figure 4c); white open circle: Linhe radar site. Gray line: 1500-m elevation ASL (northern outline: Lang Mountain). (b, c) Temperature and BLCL distributions on both sides of the oasis−desert border. Horizontal axis: distance from border (negative toward desert, positive toward the oasis). Crosses: average AWS temperature at 1200 LST (left y-axis); bars: number of BLCLs (right y-axis). The difference between the two temperature gradients (4.8℃/100 km for Kubuqi vs. 2.9 ℃/100 km for Ulan Buh) is significant (t-test $p < 0.001$). Empty arrow in (a): background wind.

Huang et al. (2019) found that 60 BLCLs form each summer in the Hetao area, with 44% initiating convection. This paper quantitatively analyzes differences in frequency, lifespan, and morphology of BLCLs over the Kubuqi and Ulan Buh deserts and their associated physical environments.

2. Data and Methods

2.1 Radar-based BLCL database

The BLCL database covers June−August 2012−2022, based on CD-band China

New Generation Doppler Weather Radar at Linhe (location given in Figure 1a). Data from 2012−2016 are from Huang et al. (2019). The database uses composite reflectivity from the two lowest elevation angles (0.5° and 1.5°) of the Linhe radar to identify BLCLs at formation, maturation, convection initiation (if present) and dissipation. Following Huang et al. (2019), a BLCL is defined as a linear area of enhanced radar reflectivity with a width < 10 km, length > 10 km, and duration ≥ 6 min. The enhanced reflectivity is generally −5 to 10 dBZ, or 0 to 10 dBZ when extensive clear-air echoes are present. A total of 174 oasis–desert BLCLs on the Kubuqi side and 47 on the Ulan Buh side were identified, with each line orienting within 45° of the vegetation border at formation and intersecting the desert sector at least once during its lifetime (Figure 1a). Of those, 88 (50.6%) on the Kubuqi side and 14 (29.8%) on the Ulan Buh side were associated with CI, suggesting stronger BLCLs on the Kubuqi side. BLCLs become increasingly frequent closer to the vegetation border (Figure 1b&c).

2.2 Vegetation and Environment Fields

The enhanced vegetation index (EVI), derived from near-infrared, red, and blue surface reflectance, was used to distinguish arid and vegetated surfaces. Following Huang et al. (2019), areas with EVI values below 0.15 were classified as arid, whereas areas with EVI values above 0.30 were classified as vegetated.

The European Centre for Medium-Range Weather Forecasts (ECMWF) ERA5 reanalysis (Hersbach et al. 2023a, b) and surface Automatic Weather Station (AWS) observations are used to examine environmental features of BLCLs. Based on evaluation of ERA5 versus AWS (details given in Text S1 and Figures S1−S3), we used AWS observations to calculate near-surface temperature and moisture gradients, because ERA5 underestimates local desert–oasis thermal and moisture contrasts. The hourly desert–oasis temperature gradient over June–August 2012–2022 was calculated as $(\overline{T_D} - \overline{T_O})/\overline{D}$, where $\overline{T_D}$ and $\overline{T_O}$ denote the average 2-m temperatures of selected AWS stations located in the desert and oasis, respectively, and $\overline{D}$ denotes the distance between the mean location of desert and oasis stations. Due to the scarcity of AWS wind observation over the desert and the decent representativeness of ERA5-Land 10-m winds for the large-scale wind and its variability in the study area, hourly ERA5-Land 10-m winds for the same period as the temperature gradient were averaged over 105°–109° E and 39°–42° N to represent background wind. The final prevailing background wind is derived by first obtaining a daily wind vector from the medians of the two horizontal components of the background wind during 0800–1800 LST, then taking the medians of each component across all days (white arrow in Figure 2a). The mean ERA5-Land 10-m wind during 0800–1800 LST in the same period is also plotted in Figure 2a showing spatial heterogeneity.

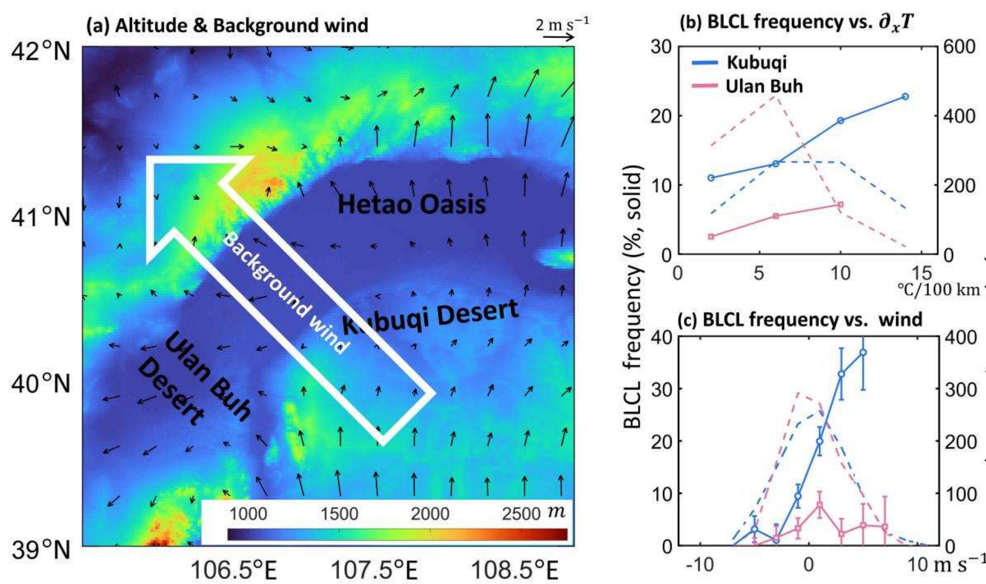

Figure 2. BLCL formation likelihood vs. temperature gradient and daytime background wind. (a) Altitude (m, ASL), the mean ERA5-Land 10-m wind during 0800–1800 LST in JJA 2012–2022 (black vectors), and the regional mean background-wind direction (the white arrow). (b) Kubuqi (blue) and Ulan Buh (pink) BLCL frequency (number of BLCL days / total days per bin, left y axis) as a function of the daily maximum desert–oasis temperature gradient. Dashed curves: the total number of days in each bin (right y axis), indicating sample size. (c) Same as (b), but as a function of the 0800–1800 LST median cross-border background wind speed (positive: cross-border wind from desert to oasis; negative: from oasis to desert). The vertical error bars in (c) show how daytime wind variability affects the estimated BLCL frequency with 90% uncertainty from Monte Carlo

resampling. A day's median wind doesn't capture hourly variation, which may misassign the day to a wrong wind bin and alter BLCL frequency. Details of the error bar estimation are given in Text S2.

3. Results

The differences in BLCLs at the two vegetation borders manifest in three aspects: frequency, lifespan, and curvature. Radar observations indicate that the BLCLs typically extend to approximately 700–1000 m AGL, with contributing factors originating primarily from the lower PBL. According to Shokurov et al. (2024), the main influencing factors of BLCLs include land surface differences, large-scale background winds, Earth's rotation, and atmospheric stratification. Because the desert–oasis area is relatively small, Earth's rotation is not significant. Therefore, this study primarily investigates the roles of thermal conditions and large-scale background winds. Many Ulan Buh BLCLs in this study occur over the transition zone between desert and oasis. Therefore, any subsequent description of "Ulan Buh Desert" properties refers to those of the transition zone.

3.1 Frequency differences

The 174 BLCLs on the Kubuqi side during 2012–2022 mainly form over Kubuqi Desert near the vegetation border (Figure 1a), while the 47 BLCLs on the Ulan Buh side are more scattered, with many in the transitional zone (Figure 1a). Moreover, 50% of Kubuqi BLCLs trigger convection, compared to only 30% on the Ulan Buh side, suggesting stronger lifting on the Kubuqi side. Although Kubuqi Desert has a much longer border length than Ulan Buh Desert, most Kubuqi BLCLs are concentrated near the western part rather than uniformly along the entire border. Actually, the active BLCL-producing length over Kubuqi Desert is comparable to that of Ulan Buh Desert (Figure S4). Even though the longer border of Kubuqi Desert does not determine the higher frequency of BLCLs, it may play an important role in their longer length.

The higher BLCL frequency on the Kubuqi side is associated with the greater temperature gradient across the oasis–Kubuqi Desert border (Figure 1b&c). Although the average temperature difference between the centers of the Kubuqi and Ulan Buh deserts and the Hetao Oasis is similar, the oasis−Ulan Buh temperature gradient is only about half that on the Kubuqi side (Figure 1b&c, Figure 2b). This is consistent with previous studies that the differential heating across a heterogeneous vegetation surface is the main driver of secondary thermal circulation and associated BLCLs (Mahfouf et al. 1987; Segal et al. 1988; Avissar and Pielke 1989; Doran et al. 1995).

The second major factor influencing BLCL frequency is background wind. Many studies have examined thermal circulation under varying background winds (Estoque, 1962; Bechtold et al., 1991; Arritt et al., 1993; Rochetin et al., 2017; Lee et al., 2019; Azorin-Molina et al., 2019). The rule of thumb is that BLCLs are more likely under weak winds from arid regions (cross-border winds from the desert are defined as positive in this paper, while along-border winds are not considered). More specifically, Bechtold et al. (1991) showed that the thermal circulation weakens when the opposing background wind becomes stronger than its low-level branch. This is because weak desert background winds strengthen dynamic convergence with the opposing low-level flow of the thermal circulation, forcing the BLCL to remain over the desert–oasis boundary where it undergoes continuous heating. By contrast, strong background winds diminish the surface temperature gradient, while oasis winds impede the upper-level return branch of the thermal circulation; both effects disrupt the circulation's structure and weaken BLCLs (Estoque, 1962).

In this region, the dominant background wind is southeasterly, roughly perpendicular to the Kubuqi−oasis border but nearly parallel to the Ulan Buh−oasis border (the white arrow in Figure 2a). In particular, the projected cross-border wind distributions in Figure 2c show more days with desert synoptic background winds on the Kubuqi side and more days with oasis winds on the Ulan Buh side, consistent with the spatial distribution of the mean ERA5-Land 10-m wind during 0800–1800 LST in

JJA 2012–2022 (black vectors in Figure 2a). Therefore, wind conditions in the Kubuqi region are slightly more favorable for BLCL formation. However, this is only part of differences in background wind influence between the two sides.

The background wind speed also differs in its relationship with BLCL occurrence. As mentioned, strong desert background winds are unfavorable for BLCL formation, which fits well on the Ulan Buh side. BLCL frequency over Ulan Buh shows only a modest peak when the cross-border background flow becomes positive at 2–3 $m\ s^{-1}$and then decreases as the desert-to-oasis background wind strengthens (Figure 2c). However, even under strong desert background winds, Kubuqi BLCLs are even more likely to form. When cross-border wind speed ranges from –4 to 4 $m\ s^{-1}$, Kubuqi BLCL frequency is nearly the same as Ulan Buh BLCL frequency at each wind speed. However, when wind speed exceeds 4 $m\ s^{-1}$, differences between the two sides become apparent. Frequency over Ulan Buh gradually decreases, as observed in large eddy models (Arritt et al., 1993; Lee et al., 2019), but frequency over Kubuqi increases.

A plausible hypothesis for the different trends in BLCL frequency with increasing background wind can be drawn from regional topography. Under typical conditions, southeasterly winds prevail over Kubuqi Desert (Figure 2a). Hourly evolution of the background 10-m wind component perpendicular to the oasis−desert border on Kubuqi BLCL days exhibits no apparent wind changes, especially no apparent decrease around the formation period of BLCLs near noon (D1 in Figure S5). Actually, the daytime variation of background winds is within the error bar of Figure 2c, where the changes associated with daytime variation are less than the range of background wind speed over Kubuqi Desert. Rather than diurnal variation, the blocking effect of Lang Mountain may play a more important role. Figure S5 shows that the background wind is weaker when averaged over a domain closer to Lang Mountain (D2) with a larger reduction under high wind conditions, which is consistent with mountain blocking in the literature (e.g., Hsiao et al. 2021). The reduction in wind speed over the thermal circulation is also clearly seen in the AWS observations (Figure S6), where the cross-border wind speed at the oasis station on the Kubuqi side is systematically weaker than that at the corresponding desert station under southerly background flow (Figure S6b, upper right quadrant). However, this wind asymmetry is not seen on the Ulan Buh side (Figure S6c). These results suggest that mountain blocking may weaken the background wind near the Kubuqi desert–oasis border and help maintain conditions favorable for BLCL formation. The detailed mechanism of the impact of Lang Mountain on BLCL activities awaits systematic numerical experiments.

In summary, the approximately threefold higher BLCL frequency on the Kubuqi side is associated with a larger desert–oasis temperature gradient and more favorable background-wind conditions.

3.2 Lifespan and location differences

Analyses based on 6-min radar observations show that the lifespan differences between the two sides manifest in duration and spatial distribution. BLCLs on both sides form in the morning and dissipate at sunset (Figure 3a&b), but Kubuqi BLCLs form 1 hour 12 minutes earlier than those on the Ulan Buh side and persist for an additional hour. This indicates that conditions on the Kubuqi side are more conducive to BLCL formation, requiring less energy accumulation after sunrise. The minimum temperature gradient occurs at 1800 LST on both sides (Figure 4a), resulting in the same average dissipation time (1800 LST).

The earlier formation of Kubuqi BLCLs is attributable to the desert's faster post-sunrise warming. Figure 4b shows that Kubuqi reaches its daily maximum temperature near 1500 LST, Ulan Buh peaks about an hour later, and the oasis peaks around 1700 LST. As a result, the desert−oasis temperature gradient over Kubuqi rises sooner and more steeply than the Ulan Buh gradient (Figure 4a). This difference is better understood from the perspective of surface energy partitioning. We compared the Bowen ratio over

Kubuqi Desert, Ulan Buh Desert, and the oasis from 1 June to 10 August 2022 (details given in Text S3). Results show that the Bowen ratio over Kubuqi Desert nearly doubles that over Ulan Buh Desert and is six times larger than that over the oasis during most daytime hours (Figure 4c), indicating that surface energy over Kubuqi Desert is more strongly partitioned into sensible heat. This enhanced sensible heating favors faster post-sunrise warming over Kubuqi Desert and supports a more rapid increase in the Kubuqi−oasis temperature gradient, favoring the earlier formation of Kubuqi BLCLs.

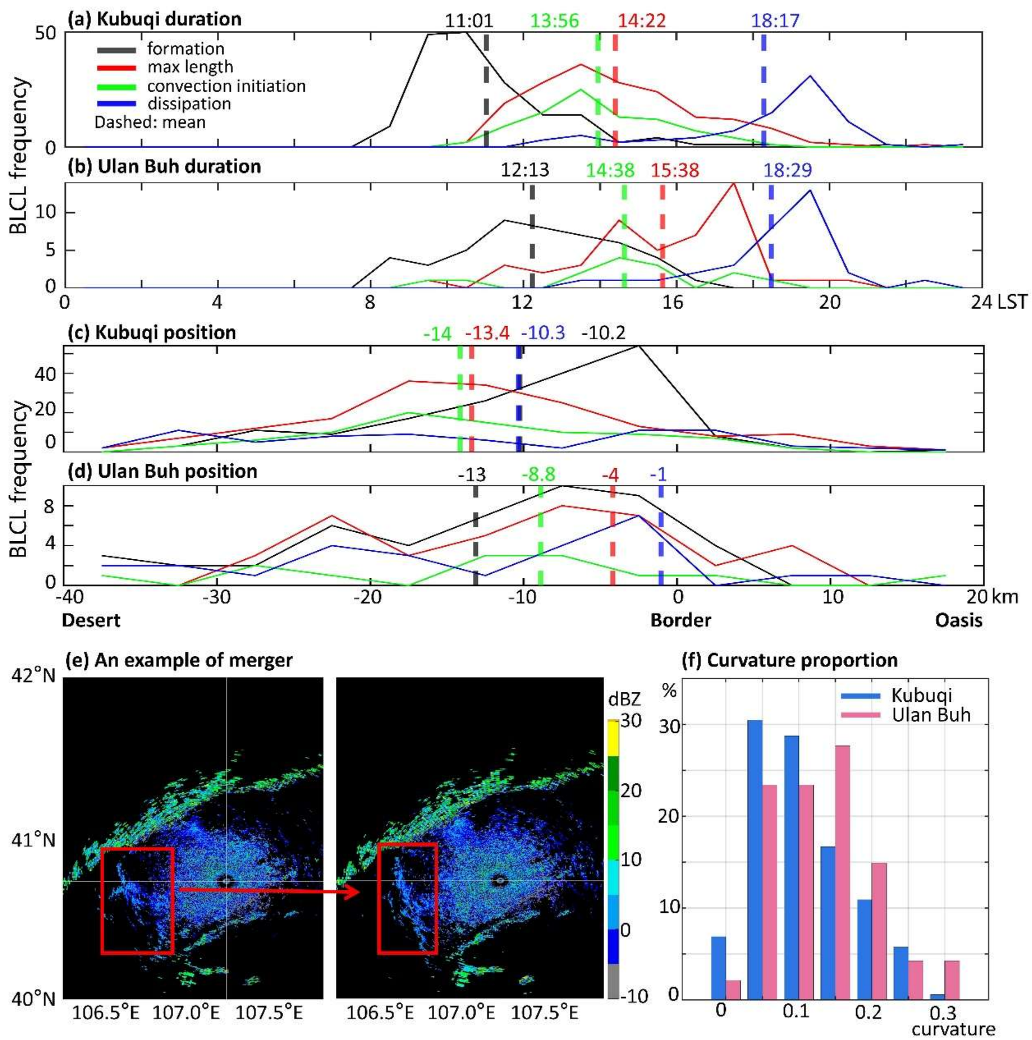

Figure 3. Diurnal distributions of BLCL occurrence frequency at key stages (formation, maximum length, convection initiation, and dissipation) on the Kubuqi (a) and Ulan Buh (b) sides. Vertical dashed lines: mean time of each stage. (c, d) Same as (a, b) but for the spatial distributions of BLCL centroid positions. The x-axis is distance relative to the oasis−desert border (0 km at border,

negative toward desert, positive toward oasis). Dashed vertical lines with numbers indicate mean positions. (e) Examples of two Ulan Buh BLCLs merging into a stronger one in 0.5° elevation radar reflectivity. Green echoes in the north indicate terrain clutter from Lang Mountain. (f) Curvature of BLCLs at maximum length for Kubuqi and Ulan Buh, with proportion of curvature bins. The curvature difference between the two deserts is statistically significant (t-test $p = 0.03$).

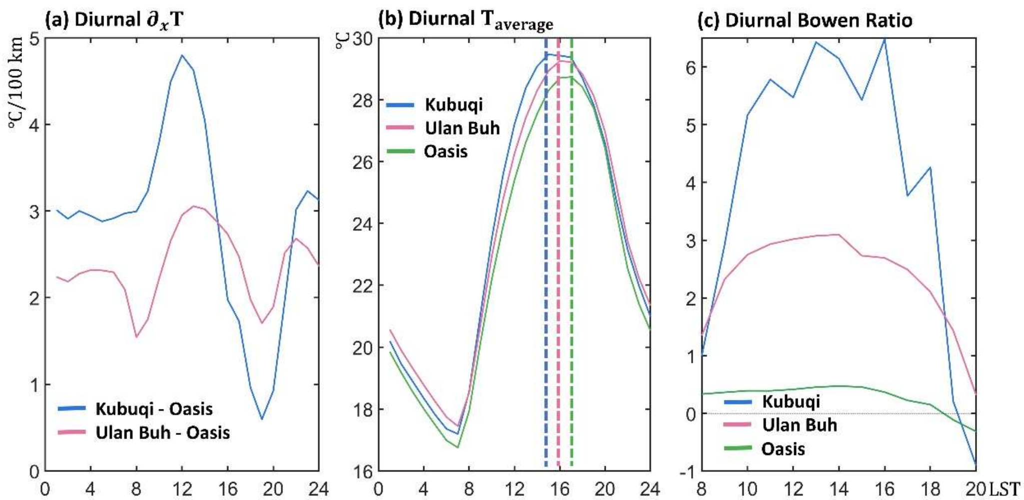

Figure 4. Mean diurnal variation of (a) desert–oasis temperature gradient for the Kubuqi and Ulan Buh deserts, (b) 2-m temperature over the two deserts and the oasis. (c) Diurnal variation of the Bowen ratio over Kubuqi Desert at site B, Ulan Buh Desert at site U, and the oasis at site A (locations given in Figure 1a). All panels are averages from 1 June to 10 August 2022.

The spatial evolution of BLCLs perpendicular to the vegetation border is illustrated in Figure 3c&d through the composite distributions of BLCL centroid positions relative to the desert–oasis border (denoted by 0 on the x-axis) for different stages of the BLCLs (denoted by different colors). In contrast to classic sea breezes, which can penetrate inland up to 150 km (Shokurov et al., 2024), oasis–desert BLCLs migrate much more slowly and rarely move beyond 40 km from the border. On the Kubuqi side, the mean positions show that BLCLs tend to form (dashed black) ~10 km into the desert from the border and propagate ~ 5 km farther into the desert, reaching maximum length (dashed red) or initiating convection (dashed green). Positions corresponding to dissipation time (dashed blue), primarily representing BLCLs that do not initiate convection, are located closer to the oasis on average. This pattern is consistent with weaker development of non-CI BLCLs, which may be more strongly affected by the prevailing southerly background flow before dissipation. In contrast, BLCLs that initiate convection generally extend farther into the desert, suggesting stronger thermally driven propagation. On the Ulan Buh side, BLCLs deviate more from the conventional picture of thermally driven convergence lines, such as sea breezes. They tend to form slightly farther into the desert and propagate toward the oasis, covering a much longer distance from formation to CI or dissipation. Both the mean positions of maximum length and CI on the Ulan Buh side are located closer to the oasis than those on the Kubuqi side. This larger variability in BLCL positions on the Ulan Buh side is consistent with the fragmented transition-zone land surface and thus more heterogeneous thermal forcing.

3.3 Curvature differences

We noticed that BLCLs are often not "linear" but exhibit a "scallop-like" or even "zigzag" shape. We quantitatively analyzed the degree of deviation from linearity. BLCL curvature is defined as the maximum deviation distance perpendicular to the line connecting its two ends. Curvature has a weak positive correlation with length, so we compared the curvature when BLCLs reach maximum length. Results show that the average curvature on the Ulan Buh side is approximately 0.2, while on the Kubuqi side it is only 0.15 (Figure 3f), indicating Ulan Buh BLCLs are more curved.

A possible explanation for the larger curvature on the Ulan Buh side is that scattered deserts, oases, and lakes in the transitional zone form a curved vegetation border (Figure 1a). Temperature does not always increase strictly from the oasis to Ulan Buh Desert (Figure 1c). Therefore, the curved border leads to curved BLCLs. Additionally, the curved morphology may be related to their formation process. Kubuqi BLCLs tend to form by extending from an initial short line along the desert–oasis border and generally remain straight. However, on the Ulan Buh side, 14 BLCLs (~30%) form through the merging of two individual short BLCLs at different locations, resulting in larger curvature.

4. Conclusions

This study compared boundary layer convergence lines (BLCLs) along the oasis−Kubuqi and oasis−Ulan Buh borders of the Hetao region, Inner Mongolia, China, revealing marked differences in frequency, lifespan, and geometry. Kubuqi BLCLs occur roughly three times as often as their Ulan Buh counterparts and initiate more convection, indicating distinct thermal and dynamical environments at the two borders. The difference in BLCL frequency are clearly associated with the sharper vegetation contrast between oasis and Kubuqi Desert relative to that between oasis and Ulan Buh Desert, in addition to the blocking effect of Lang Mountain on the west−east oriented oasis.

Results show that the sharper vegetation contrast caused a larger temperature gradient on the Kubuqi side, playing an important role in driving BLCL formation. The localized desert−oasis gradient is nearly doubled on the Kubuqi side compared to the Ulan Buh side. This stronger gradient sets up a more pronounced thermal circulation, thereby increasing both the likelihood and the intensity of BLCLs.

Background winds also substantially influence BLCL development. In the Hetao region, southeasterly winds prevail throughout most of the summer. Kubuqi Desert experiences more days with desert background winds, whereas Ulan Buh Desert has slightly more days with oasis background winds. Therefore, the wind pattern over the Kubuqi side is more favorable for BLCL formation, consistent with previous studies. Furthermore, even under strong desert winds, Kubuqi BLCLs can still develop and persist, possibly because the blocking effect of Lang Mountain decelerates strong desert winds when they get closer to the oasis–desert border and thus fail to disrupt the oasis–desert thermal circulation.

In addition, BLCLs form earlier over Kubuqi than over Ulan Buh, attributed to Kubuqi's higher Bowen ratio, allowing faster surface warming. Kubuqi BLCLs follow a pattern: after initiation, they move into the desert interior and retain a relatively simple, linear shape. On the Ulan Buh side, however, BLCLs are more stationary, more curved, and may form through merger processes. The larger curvature on the Ulan Buh side possibly stems from the merging formation process on the one hand, and the fragmented landscape with scattered patches of desert, oasis, and lakes creating a more complex thermal structure on the other. This contrast with the more linear boundary on the Kubuqi side underscores the importance of land-cover transitions in shaping convergence line morphology. These results may provide important indications for BLCL behaviors across oasis–desert borders with various vegetation gradients in other places of the world.

Acknowledgements

This study was sponsored by the National Natural Science Foundation of China (Grants 42530601 and 42030604).

Conflict of Interest Statement

The authors have no conflicts of interest to disclose.

Open Research

The radar and AWS data were provided by the National Meteorological Information Center of the China Meteorological Administration (https://data.cma.cn/data/cdcindex/cid/0b9164954813c573.html). The MODIS data (MOD13A3-V061, (Didan, 2021)) were downloaded from NASA's Earth Observing

System Data and Information System (EOSDIS; https://search.earthdata.nasa.gov/search). The ERA5 hourly data from 2021 to 2022 on pressure levels and single levels are available respectively at Hersbach et al. (2023a, b).

References

Arritt, R. W. (1993). Effects of the Large-Scale Flow on Characteristic Features of the Sea Breeze. *Journal of Applied Meteorology and Climatology, 32*, 116–125, https://doi.org/10.1175/1520-0450(1993)032<0116:EOTLSF>2.0.CO;2

Avissar, R., & Pielke, R. A. (1989). A parameterization of heterogeneous land surfaces for atmospheric numerical models and its impact on regional meteorology. *Monthly Weather Review, 117*(10), 2113 – 2136. https://doi.org/10.1175/1520-0493(1989)117<2113:APOHLS>2.0.CO;2

Azorin-Molina, C., Chen, D. (2009). A climatological study of the influence of synoptic-scale flows on sea breeze evolution in the Bay of Alicante (Spain). *Theoretical and Applied Climatology, 96*, 249–260. https://doi.org/10.1007/s00704-008-0028-2

Bechtold, P., J. Pinty, and F. Mascart. (1991). A Numerical Investigation of the Influence of Large-Scale Winds on Sea-Breeze- and Inland-Breeze-type Circulations. *Journal of Applied Meteorology and. Climatology, 30*, 1268–1279, https://doi.org/10.1175/1520-0450(1991)030<1268:ANIOTI>2.0.CO;2

Bou-Zeid, E., Anderson, W., Katul, G.G. et al. (2020). The Persistent Challenge of Surface Heterogeneity in Boundary-Layer Meteorology: A Review. *Boundary-Layer Meteorology, 177*, 227–245. https://doi.org/10.1007/s10546-020-00551-8

C. Hohenegger, & B. Stevens. (2018). The role of the permanent wilting point in controlling the spatial distribution of precipitation, *Proceedings of the National Academy of Sciences of the United States of America*, 5692–5697, https://doi.org/10.1073/pnas.1718842115

Chug, D., Dominguez, F., Taylor, C. M., Klein, C., & Nesbitt, S. W. (2023). Dry-to-wet soil gradients enhance convection and rainfall over subtropical south America. *Journal of Hydrometeorology*, *24*(9), 1563–1581. https://doi.org/10.1175/JHM-D-23-0031.1

Didan, K. (2021). Modis/terra vegetation indices monthly L3 global 1km sin grid 650 (Version 6.1) [Dataset]. *NASA EOSDIS Land Processes DAAC,* https://doi.org/10.5067/MODIS/MOD13A3.061

Doran, J. C., W. J. Shaw, and J. M. Hubbe. (1995). Boundary layer characteristics over areas of inhomogeneous surface fluxes. *Journal of Applied Meteorology*, *34*, 559–571. https://doi.org/10.1175/1520-0450-34.2.559

Estoque MA. (1962). The sea breeze as function of the prevailing synoptic situation. *Journal of the Atmospheric Sciences, 19*, 244–250. https://doi.org/10.1175/1520-0469(1962)019<0244:TSBAAF>2.0.CO;2

Hersbach, H., Bell, B., Berrisford, P., Biavati, G., Horányi, A., Muñoz Sabater, J., Nicolas, J., Peubey, C., Radu, R., Rozum, I., Schepers, D., Simmons, A., Soci, C., Dee, D., Thépaut, J-N. (2023a). ERA5 hourly data on pressure levels from 1940 to present [Dataset]. *Copernicus Climate Change Service (C3S) Climate Data Store (CDS).* https://doi.org/10.24381/cds.adbb2d47

Hersbach, H., Bell, B., Berrisford, P., Biavati, G., Horányi, A., Muñoz Sabater, J., Nicolas, J., Peubey, C., Radu, R., Rozum, I., Schepers, D., Simmons, A., Soci, C., Dee, D., Thépaut, J-N. (2023b). ERA5 hourly data on single levels from 1940 to present [Dataset]. *Copernicus Climate Change Service (C3S) Climate Data Store (CDS).* https://doi.org/10.24381/cds.adbb2d47

Huang, Y., Meng, Z., & Zhang, M. (2022). Synoptic impacts on the occurrence of mesoscale boundaries and their associated convection over an area of sharp vegetation contrast. *Geophysical Research Letters*, *49*(16), e2022GL099449. https://doi.org/10.1029/2022GL099449

Huang, Y. P., Meng, Z. Y., Li, W. B., Bai, L. Q., & Meng, X. F. (2019). General features of radar-observed boundary layer convergence lines and their associated convection over a sharp vegetation-contrast area. *Geophysical Research Letters*, *46*(5), 2865-2873. https://doi.org/10.1029/2018gl081714

Hsiao, F., Chen, Y.-L., Nguyen, H. V., Hitzl, D. E., & Ballard, R. (2021). Effects of trade wind strength on airflow and cloudiness over Oahu. *Monthly Weather Review*, *149*(9), 3037–3062. https://doi.org/10.1175/MWR-D-20-0399.1

Kang, S., and G. H. Bryan. (2011). A Large-Eddy Simulation Study of Moist Convection Initiation over Heterogeneous Surface Fluxes. *Monthly Weather Review*, 139, 2901–2917, https://doi.org/10.1175/MWR-D-10-05037.1

Klein, C., & Taylor, C. M. (2020). Dry soils can intensify mesoscale convective systems. *Proceedings of the National Academy of Sciences of the United States of America*, *117*(35), 21132-21137. https://doi.org/10.1073/pnas.2007998117

Lee, J. M., Y. Zhang, and S. A. Klein. (2019). The Effect of Land Surface Heterogeneity and Background Wind on Shallow Cumulus Clouds and the Transition to Deeper Convection. *Journal of the Atmospheric Sciences*, 76, 401–419, https://doi.org/10.1175/JAS-D-18-0196.1

Liu, H., Meng, Z., Zhu, Y., & Huang, Y. (2023). Convection initiation associated with a boundary layer convergence line over a real-world sharp vegetation-contrast area. *Monthly Weather Review*, *151*(5), 1189–1212. https://doi.org/10.1175/MWR-D-22-0083.1

Mahfouf, J. F., Richard, E., & Mascart, P. (1987). The influence of soil and vegetation on the development of mesoscale circulations. *Journal of Climate and Applied Meteorology*, *26*(11), 1483 – 1495. https://doi.org/10.1175/1520-0450(1987)026<1483:TIOSAV>2.0.CO;2

Meng, Z. Y., et al. (2024). Desert Oasis Convergence Line and Deep Convection Experiment (DECODE). *Bulletin of the American Meteorological Society,* 105(12), E2355–E2384. https://doi.org/10.1175/BAMS-D-23-0222.1

Rieck, M., C. Hohenegger, and C. C. van Heerwaarden. (2014). The Influence of Land Surface Heterogeneities on Cloud Size Development. *Monthly Weather Review*, 142, 3830–3846, https://doi.org/10.1175/MWR-D-13-00354.1

Rochetin, N., Couvreux, F., & Françoise Guichard. (2017). Morphology of breeze circulations induced by surface flux heterogeneities and their impact on convection initiation. *Quarterly Journal of the Royal Meteorological Society, 143*(702).463–478. https://doi.org/10.1002/qj.2935

Segal, M., Avissar, R., McCumber, M. C., & Pielke, R. A. (1988). Evaluation of vegetation effects on the generation and modification of mesoscale circulations. *Journal of the Atmospheric Sciences, 45*(16), 2268 – 2292. https://doi.org/10.1175/1520-0469(1988)045<2268:EOVEOT>2.0.CO;2

Shokurov, M.V. and Kraevskaya, N.Yu. (2024). Sea Breeze Circulation: Theory and Two-Dimensional Simulation (Review). *Physical Oceanography*, 31(4), 447–466.

NASA/METI/AIST/Japan Spacesystems and U.S./Japan ASTER Science Team. (2019). Aster global digital elevation model v003 [Dataset]. *NASA EOSDIS Land Processes DAAC*. https://doi.org/10.5067/ASTER/ASTGTM.003

Wilson, J. W., Weckwerth, T. M., Vivekanandan, J., Wakimoto, R. M., & Russell, R. W. (1994). Boundary layer clear-air radar echoes: Origin of echoes and accuracy of derived winds. *Journal of Atmospheric and Oceanic Technology, 11*(5), 1184–1206. https://doi.org/10.1175/1520-0426(1994)011<1184:BLCARE>2.0.CO;2

Yuan, S. S., Wang, Y. C., Quiring, S. M., Ford, T. W., & Houston, A. L. (2020). A sensitivity study on the response of convection initiation to in situ soil moisture in the central united states. *Climate Dynamics*, *54*(3–4), 2013–2028. https://doi.org/10.1007/s00382-019-05098-0

Geophysical Research Letters

Supporting Information for

Contrast in the Boundary Layer Convergence Lines at Desert–Oasis Border with Different Vegetation Gradient

Zimeng Zheng[1], Zhiyong Meng[1*], Quxin Cui[1], Yipeng Huang[2], Xuefeng Meng[3]

[1]Department of Atmospheric and Oceanic Sciences, School of Physics, and China Meteorological Administration Tornado Key Laboratory, Peking University, Beijing, China

[2]Xiamen Key Laboratory of Straits Meteorology, Xiamen Meteorological Bureau, Xiamen, China

[3]Inner Mongolia Meteorological Observatory, Hohhot, China

Contents of this file

Text S1 and S3
Figures S1 to S7

Introduction

This document includes the following materials:

- **Text S1 and Figure S1-S3:** Evaluation of ERA5 against AWS observations;
- **Text S2** Error bar estimation of BLCL frequency as a function of the daytime median cross-border background wind speed.
- **Figure S4:** Observational evidence of slowed cross-border wind at an oasis site relative to a Kubuqi desert site;
- **Figure S5**: Diurnal variation of the background wind;
- **Figure S6**: Active length of oasis–desert border for BLCL formation.;
- **Text S3 and Figure S7:** Evaluation of Bowen-ratio estimation over Ulan Buh Desert using ERA5 due to data limitation.

Text S1. Evaluation of ERA5 against AWS observations

We evaluated whether ERA5 can represent near-surface temperature, humidity, and the corresponding desert–oasis contrasts in the Hetao region. Figure S1 compares co-located AWS observations and ERA5 fields for 2-m temperature, 2-m specific humidity, and their desert–oasis differences. ERA5 represents regional 2-m temperature reasonably well but shows systematic biases in 2-m humidity and strongly underestimates the local desert–oasis thermal and moisture contrasts. Figure S2 further shows that the positive relationship between BLCL frequency and desert–oasis temperature gradient appears when the gradient is calculated from AWS observations, but nearly disappears when the gradient is calculated from ERA5. Therefore, AWS observations are used in the main text to calculate near-surface temperature and moisture gradients.

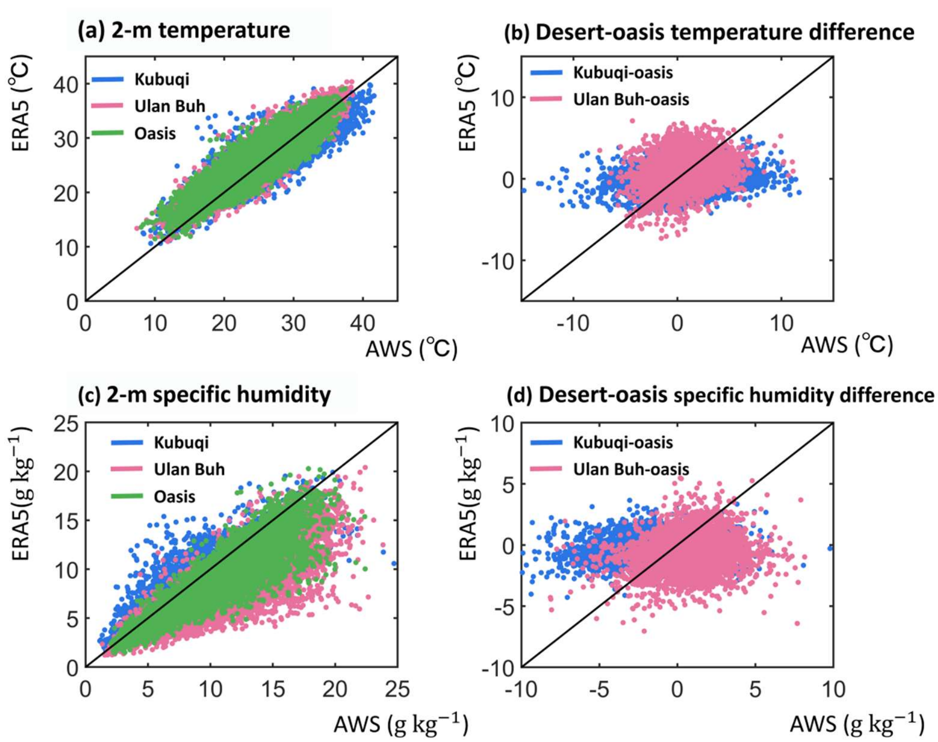

Figure S1. Comparison between local AWS observations and co-located ERA5 reanalysis for the two deserts and the oasis. The x-axis gives AWS value, the y-axis ERA5 value, and the solid black line denotes the 1:1 relationship. (a) and (c) illustrate ERA5 biases in 2-m temperature and 2-m specific humidity. (b) and (d) display the large underestimate of desert–oasis differences in ERA5 data.

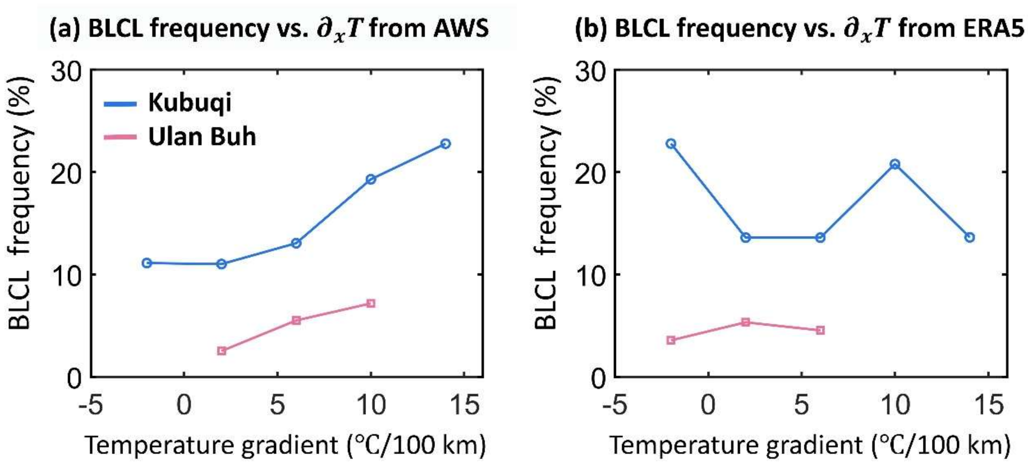

Figure S2. Frequency of BLCLs (ratio of BLCL days to total days in each bin) as a function of daily maximum desert–oasis 2-m temperature gradient, derived from (a) AWS observations and (b) ERA5 reanalysis. Panel (a) shows a clear positive correlation between BLCL frequency and temperature gradient in AWS data, whereas panel (b) indicates little to no correlation in ERA5, implying that ERA5 fails to adequately capture the local surface heterogeneity in this region.

Surface wind observations from AWS stations are limited over Kubuqi Desert. During 2012–2019, only one AWS station over Kubuqi Desert measured near-surface wind. We compared available AWS wind observations with co-located ERA5-Land winds during 2020–2022 (Figure S3). The comparison shows that ERA5-Land captures the main large-scale wind variability reasonably well, although local biases remain. Therefore, ERA5-Land 10-m winds are used in the main text to represent the synoptic background wind.

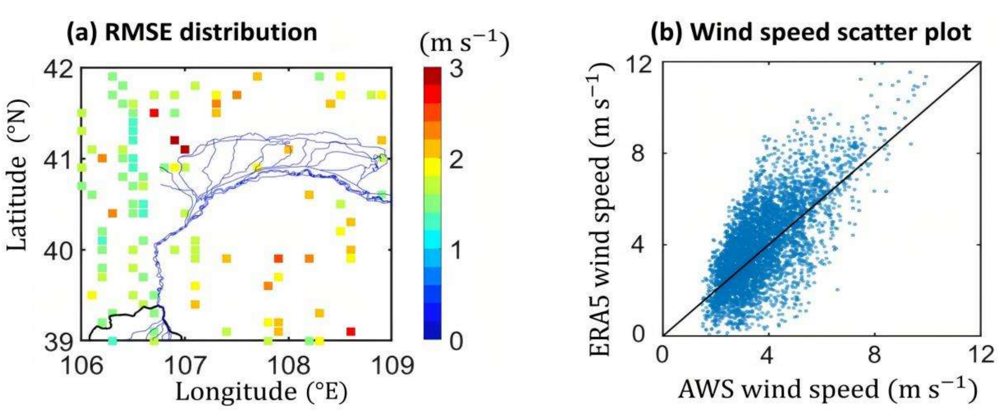

Figure S3. Evaluation of ERA5 10-m winds against AWS observations during 2020–2022. Data from 2012–2019 are excluded due to lack of continuous AWS wind measurements. Panel (a) shows spatial distribution of root-mean-square error (RMSE) between hourly AWS wind speeds and corresponding ERA5-Land grid-point values (0.1° resolution), after mapping each AWS station to its nearest ERA5-Land grid point. At most stations, RMSE values remain below 2 m s^{-1}. Panel (b) shows scatterplot comparison of hourly 10-m wind speeds from AWS and ERA5-Land. Although systematic biases are evident, most data points lie close to the 1:1 relationship. These results suggest ERA5-Land provides reasonable representation of large-scale background wind variability in the study area.

Text S2. Error bar estimation of BLCL frequency as a function of the daytime median cross-border background wind speed.

Although the median value is used as the daily representative, wind speed varies considerably within the 0800–1800 LST period. This intra-day variability introduces uncertainty that ultimately manifests as vertical error bars on the BLCL frequency.

The key mechanism is bin assignment. Each day is assigned to a wind-speed bin based on its 0800–1800 LST median wind. However, because the wind fluctuates hour by hour, the same day could fall into a neighboring bin if a different moment of the daytime period were considered. Consequently, uncertainty in the x-axis variable (background wind) propagates through binning and alters the BLCL frequency calculated for each bin.

To quantify this effect, we performed a Monte Carlo simulation with 5000 realizations for each day from June–August, 2012–2022. For each realization, we perturbed the daily 0800–1800 LST median wind speed by adding random noise drawn from a Gaussian distribution with the standard deviation of hourly wind speeds observed during 0800–1800 LST on that day, representing the actual intra-day variability. Each perturbed value was then treated as a simulated daily median wind, and the entire binning and frequency calculation procedure was repeated exactly as for the original data.

After all 5000 realizations, each wind-speed bin yielded 5000 possible BLCL frequency values. We took the 5th and 95th percentiles of this distribution as the lower and upper bounds of the 90% uncertainty range, which are plotted as the error bars in Figure 2c.

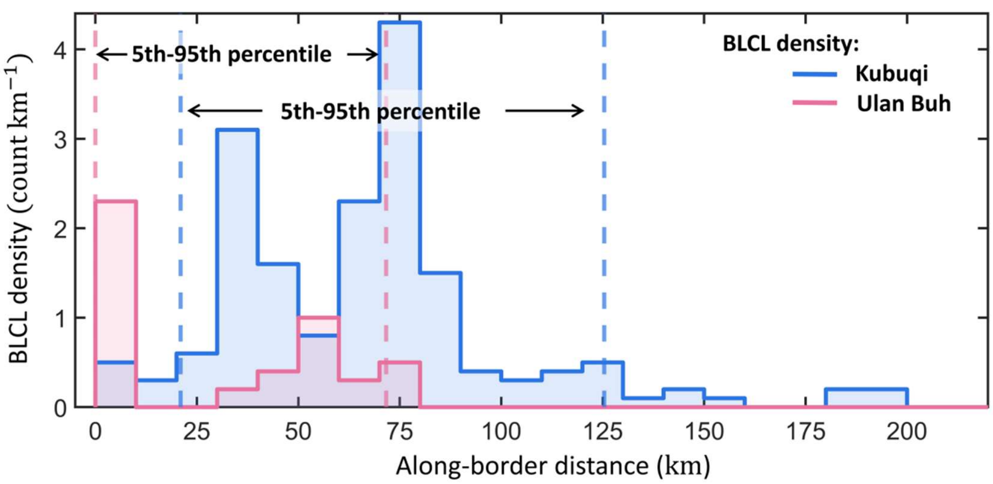

Figure S4. Probability density distribution of BLCL centroid positions along the oasis–desert border at the formation time on the Kubuqi side and the Ulan Buh side. The dashed vertical lines denote the 5th and 95th percentiles of BLCL centroid positions. On the Kubuqi side, about 90% of BLCL centroids are distributed within approximately 104 km along the border, although the total border length extends to nearly 212 km. On the Ulan Buh side, about 90% of BLCL centroids are distributed within approximately 72 km.

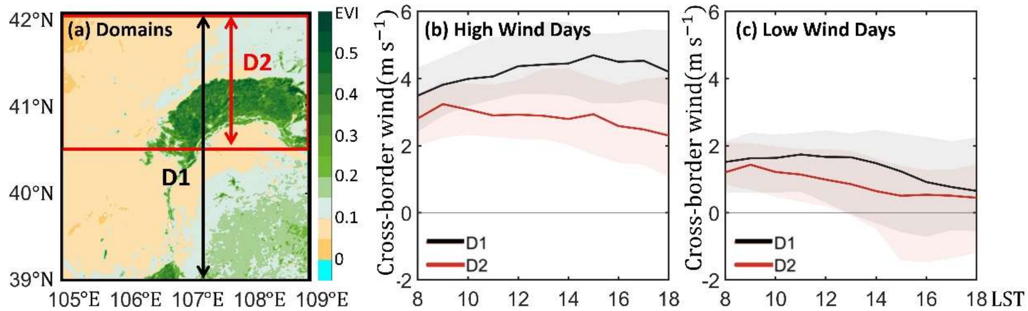

Figure S5. Spatial and temporal variations of the background wind component normal to the Kubuqi desert–oasis border on BLCL days. (a) Domains used to calculate background wind using ERA5. The shading denotes EVI. D1 is the whole domain, while D2 is the domain closer to the oasis and Lang Mountain. (b) Diurnal variation of the cross-border background wind during 0800−1800 LST on Kubuqi BLCL days for high wind days. (c) Same as (b) but for low wind days. High and low wind days are classified using the daily 0800−1800 LST median cross-border background wind component averaged over D1, with a threshold of 3 m s^{-1}. Shading indicates the interquartile range. Positive values denote flow from Kubuqi Desert to the oasis.

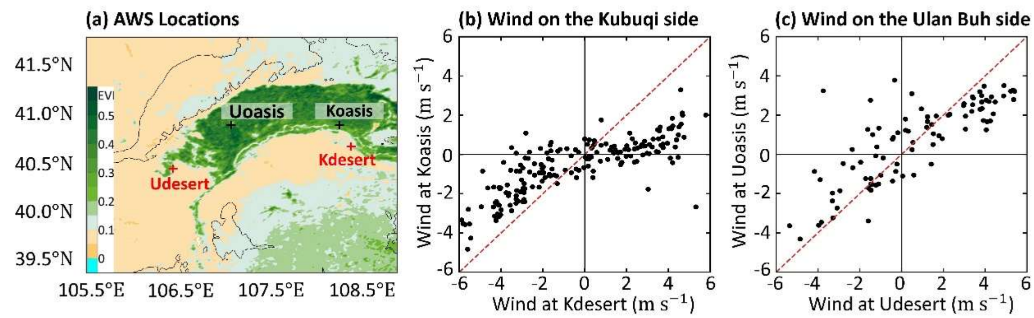

Figure S6. Comparison of cross-border wind speed measured at (a) a desert and an oasis AWS station at Koasis and Kdesert across the Kubuqi-oasis border, and Uoasis and Udesert across the Ulan Buh desert–oasis border (a) during 0800–1800 LST from June–Aug 2021–2022. The red dashed line denotes the 1:1 relationship. On the Kubuqi side (b), the oasis-side cross-border wind is systematically weaker than the desert-side cross-border wind, indicating a strong reduction of low-level inflow toward the oasis–desert border. On the Ulan Buh side (c), this contrast is much weaker.

Text S3. Evaluation of Bowen-ratio estimation over Ulan Buh Desert using ERA5 due to data limitation.

The eddy-covariance observations were collected at Kubuqi site B and oasis site A (locations given in Figure 1a) from 1 June to 10 August 2022, whereas the Ulan Buh observations were collected at site U (location given in Figure 1a) from 17 to 31 August 2022. We therefore evaluated ERA5 against the Ulan Buh observations during 17–31 August 2022 (Figure S7). Although ERA5 somewhat underestimated the daytime peaks, it decently captured the daytime evolution of Bowen ratio. We thus used ERA5 to estimate the Ulan Buh Bowen ratio from 1 June to 10 August 2022, matching the Kubuqi observation period. The underestimation does not affect the main conclusion, because the Bowen ratio over Kubuqi Desert almost doubles that over Ulan Buh Desert and six times larger than that over the oasis during most daytime hours (Figure 4c).

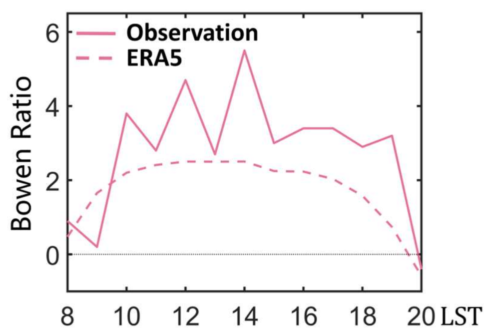

Figure S7. Comparison between the observed Bowen ratio at the Ulan Buh site U (location given in Figure 1a) and the ERA5 estimated Bowen ratio interpolated to the same location during 17–31 August 2022.